ADVANCED FUNCTIONAL MATERIALS
www.afm-journal.de

Discotic Liquid Crystal-Functionalized Gold Nanorods: 2- and 3D Self-Assembly and Macroscopic Alignment as well as Increased Charge Carrier Mobility in Hexagonal Columnar Liquid Crystal Hosts Affected by Molecular Packing and π–π Interactions

*Xiang Feng, Lydia Sosa-Vargas, S. Umadevi, Taizo Mori, Yo Shimizu, and Torsten Hegmann**

Gold nanorods functionalized with triphenylene-based discotic liquid crystal (LC) motifs show striking self-assembly behavior both on transmission electron microscopy (TEM) grids as well as in the bulk enforced by the π–π-stacking of triphenylene groups of adjacent nanorods. TEM images confirm that these discotic LC nanorods form ribbons of parallel-stacked nanorods several hundred nanometer long. The pursued silane conjugation approach to decorate the nanorods allows for the preparation of dispersions of the nanorods in the hexagonal columnar phases of parent discotic LCs, where the nanorods can be macroscopically aligned with almost 80% efficiency by a simple shearing protocol. Doping the parent host materials with about 1% by weight of the discotic LC-capped nanorods also reduces the lattice parameter and the intracolumnar packing, which gives rise to enhanced charge carrier mobility in these hosts as determined by time-of-flight measurements.

1. Introduction

Approaches of manipulating anisotropic nanoparticles, in order to arrange the particles into ordered assemblies,[1] generated significant interest over the past few years for the creation of metamaterials,[2] for optical applications, such as high efficiency polarizers[3] and display applications,[4] as well as for applications in surface-enhanced Raman spectroscopy.[5] However, the assembly and manipulation of anisotropic building blocks into complex superstructures is still a challenging task in comparison to their corresponding quasi-spherical counterpart nanoparticles.[6] The key-limiting factor most often described is the irreversible aggregation of the anisometric nanomaterial in a given fluid or polymer host medium. It is well understood that the interactions between nanostructures plays a critical role during the self-assembly process.[7] Ionic additives[8] or cationic surfactants[9] have been employed to tune the attraction between nanoparticles in colloidal suspensions and improve the ability of inducing nanorods assemblies.

In an earlier paper, we reported a fascinating large-area self-assembly of nematic liquid crystal (LC)-functionalized gold nanorods (GNRs) forming nematic- and smectic-like patterns on substrates, and nematic-phase behavior in the bulk.[10] The interaction between the LC molecules attached to the surface of the GNRs was established as the driving force for the self-assembly of such GNRs. The attached LC ligands tended to pack together next to each other when the GNRs dispersion became more and more concentrated during solvent evaporation, and attractive interactions between the capping LC ligands facilitated the formation of large-area nematic and smectic superstructures of the GNRs. To extent this concept to higher ordered LC phases that would facilitate long-range order, alignment, and even enhanced photoconductivity, we here present the synthesis, characterization, as well as the surface and bulk self-assembly of GNRs functionalized with discotic triphenylene-based LC (DLC) molecules (**Figure 1**a). Strong π–π interactions between the triphenylene cores should aid the self-assembly as well as integration and alignment in structurally identical triphenylene hosts. Yamada et al.[11] reported a 2D hexagonal superstructure of such DLC-functionalized gold nanoparticles on the substrate of transmission electron microscopy

X. Feng, Dr. S. Umadevi,[+] Prof. T. Hegmann
Department of Chemistry
University of Manitoba
Winnipeg, Manitoba R3T 2N2, Canada
E-mail: thegmann@kent.edu
Dr. L. Sosa-Vargas, Prof. Y. Shimizu
Nanotechnology Research Institute
National Institute of Advanced Industrial
Science and Technology (AIST)
Ikeda, Osaka, Japan
Dr. T. Mori, Prof. T. Hegmann
Liquid Crystal Institute and Chemical Physics
Interdisciplinary Program
Kent State University
Kent, OH 44242, USA
Prof. T. Hegmann
Department of Chemistry & Biochemistry
Kent State University
Kent, OH 44242-0001, USA
[+]Present address: Department of Industrial Chemistry, Alagappa University, Karaikudi-630 003, India

DOI: 10.1002/adfm.201401844

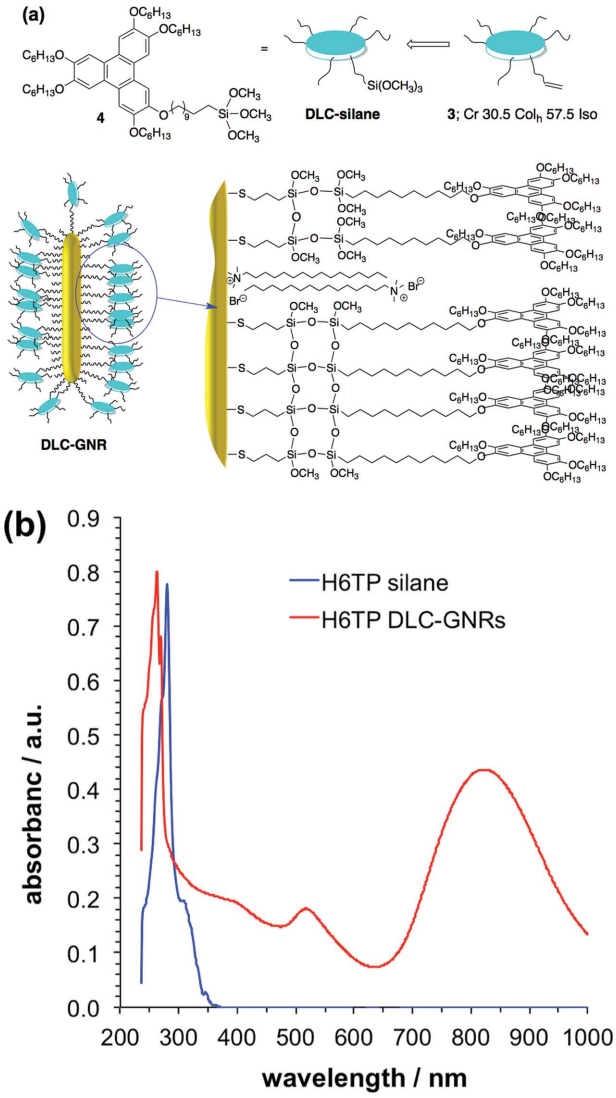

Figure 1. a) Structure and phase-transition temperatures of the DLC silane precursor **3** and silane **4** as well as a 2D schematic representation of the DLC-functionalized GNRs (**DLC-GNR**). b) UV–Vis–NIR spectra of the DLC silane **4** and the **DLC-GNR**s.

(TEM) grids after solvent evaporation. The authors concluded that the packing status of the functional LC ligands in the dispersion influenced the self-assembly of the nanoparticles on TEM grids. Kumar and co-workers[12] presented data on such DLC nanocomposites, which show that DLC-functionalized gold nanoparticles[12a] and modified carbon nanotubes[12b] enhance the electrical conductivity of the DLC hosts to a very high level compared with the pure DLC. The authors also suggested that the inclusion of shape-anisotropic nanotubes into the DLC matrix leads to a homogeneous dispersion of the nanotubes in the DLC superlattice, and predicted that alignment of 1D nanostructures can be achieved by employing well-established LC-alignment technologies.

Herein, we describe for the first time GNRs functionalized with DLC molecules via a silane conjugation approach,[13] the self-assembly in the bulk and on TEM grids as well as their alignment in the superlattices of the parent DLC host in planar alignment cells and the effect of the GNR inclusions on the charge carrier mobility of the DLC host.

2. Experimental Section

General Methods: All chemicals were obtained from commercial sources ($HAuCl_4 \cdot 3H_2O$, $AgNO_3$, ascorbic acid, $NaBH_4$, cetyltrimethylammonium bromide (CTAB), B-bromocatecholborane, Karstedt's catalyst, octadecyltrimethoxysilane (ODS) are all purchased from Sigma-Aldrich) and used without further purification. High-purity deionized (DI) water (Millipore, 18 MΩ) and Aldrich purification grade solvents purified via a PureSolv solvent purification system (Innovative Technology, Inc.) were used for the synthesis and purification of the presented materials. All glassware used for synthesis and sample handling was cleaned with *aqua regia* and thoroughly rinsed with DI water. A highly pure sample of the LC H4TP was available in our laboratories.

UV–Vis–NIR absorption spectra were recorded using an Agilent Cary 5000 UV–Vis–NIR spectrophotometer using a quartz cell (1 cm path length). TEM images were recorded on a Hitachi H 7000 microscope. The samples were prepared by drop casting a 5 µL dispersion of the GNR solution onto carbon-coated copper grids (400 meshes) and dried overnight under ambient conditions. Polarized optical photoimages were taken using an Olympus BX51-P polarizing optical microscope equipped with a Linkam LS 350 heating/cooling stage. Small-angle X-ray diffraction (SAXD) data were collected using a Rigaku 3-pinhole camera (S-MAX 3000) equipped with a Rigaku MicroMax+002 microfocus sealed tube (Cu Kα radiation at λ = 1.54 Å) and Confocal Max-Flux optics operating at 40 W. The system has a 3 m, fully evacuated camera length, and is equipped with 200 mm multiwire 2D detector for data collection as well as an option to use image plates at various distances away from the sample. The data reduction was performed using Rigaku's SAXGUI data processing software.

Mechanical shearing was used to obtain planar alignment of the H6TP/GNRs composite in the Col$_{ho}$ phase (85 °C). The polarized UV–Vis–NIR spectrophotometry was carried at the same temperature using the same Linkam heating stage in the beam path of the spectrophotometer.

The charge carrier mobility measurements were carried out using the time-of-flight (TOF) technique by injecting a sample of the **DLC-GNR**-doped H4TP (1 and 2 wt%), **DLC-GNR**-doped H6TP (1 wt%), and undoped, high-purity H4TP into ITO-coated, sandwich-type cells (cell gap: 2–3 µm, measured by interferometry). The H4TP used for the TOF experiments was purified by successive recrystallizations in spectroscopic-grade toluene and treatment with a chelating solution (aqueous ethylenediaminetetraacetic acid) to remove ionic impurities. The samples were injected by capillary action in the isotropic phase. The TOF measurements were carried out on slow cooling from the isotropic liquid to the crystalline phase. Carrier transport was measured using the conventional TOF setup and a N_2 laser (λ = 337 nm) as the excitation source, whilst recording the photocurrents with an oscilloscope. Temperature variation was obtained with a hot-stage and temperature controller.

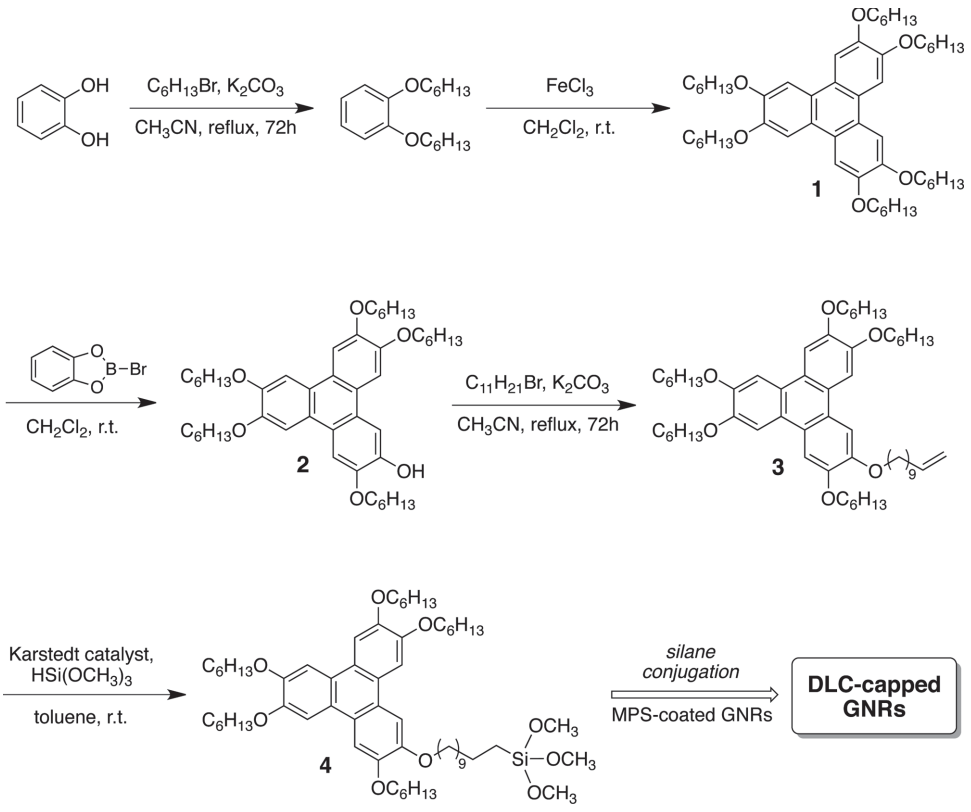

Scheme 1. Synthesis route to triphenylene LC-decorated GNRs following a silane-conjugation approach.

Homeotropic alignment of the samples was monitored by polarized optical microscopy and obtained by slow heating and cooling from the isotropic liquid phase.[14]

Synthesis: The monofunctionalized triphenylene derivatives for the conjugation to the GNRs was synthesized according to a previously published procedure,[15] and the hydrosilylation reaction was following the same conditions described in our earlier work.[10] The synthesis of the monoalkene-functionalized hexaalkoxytriphenylene (**Scheme 1**) was performed as follows:[15,16] A solution of H6TP, **1**, (0.67 g, 0.5×10^{-3} mol) in anhydrous CH_2Cl_2 (10 mL) was cooled to 0 °C before 1.2 eq. (0.12 g, 0.6×10^{-3} mol) B-bromocatecholborane (dissolved in 1 mL CH_2Cl_2) was added dropwise. The mixture was kept stirring at room temperature for 72 h. Thereafter, it was poured on ice water (50 mL), and the water layer was extracted with CH_2Cl_2 (two times 20 mL). The organic layer was separated by column chromatography (hexanes/ethyl acetate = 30/1). The purified monohydroxy triphenylene compound **2** (0.18 g, 0.24×10^{-3} mol) was dissolved in 10 mL THF, and KOH (0.0132 g, 0.24×10^{-3} mol) was added under stirring. The reaction was refluxed for 1 h before 11-bromo-1-undecene (0.174 mL, 0.8×10^{-3} mol) was injected. The system was kept under reflux for 24 h, and was then poured into 20 mL 1 M HCl, and extracted with CH_2Cl_2 (twice 20 mL). The monoalkene compound **3** (Cr 30.5 Col 57.5 Iso) was purified by recrystallization from *n*-hexane. Compound **3** (0.09 g, 0.1×10^{-3} mol) was then dissolved in 2 mL of dry toluene, and under stirring 64 µL of trimethoxysilane (0.5×10^{-3} mol) and 20 µL of Karstedt's catalyst (0.1 M in xylene) was added subsequently. The reaction was stirred at room temperature for 24 h. The monosilane compound **4** was purified by filtration through a 0.45 µm PTFE syringe microfilter before silane conjugation to the (3-mercaptopropyl)trimethoxysilane (MPS)-coated GNRs. Further details can be found in the Supporting Information.

Next, the GNRs were synthesized following the modified single-step growth method using CTAB as initial capping agent, as described earlier.[10,17] Synthesis of CTAB-GNRs: a 250 mL water solution containing the following compounds was prepared: $[HAuCl_4 \cdot 3H_2O] = 1.0 \times 10^{-3}$ M, [CTAB] = 0.20 M, $[AgNO_3] = 0.20 \times 10^{-3}$ M, [ascorbic acid] = 2.0×10^{-3} M. Then 1.87 mL of 0.1×10^{-3} M ice-cold $NaBH_4$ aqueous solution was added into the mixture under stirring. After 2 min, the mixture was kept for 24 h at 30 °C allowing the growth of the GNRs. The resulting GNRs were washed by repeated agitation with 100 mL DI water and centrifugation at 16 000 rpm for 20 min.

The functionalization of the CTAB-GNRs was achieved by a two-step silane hydrolysis–condensation reaction reported previously:[10,17,18] 3 mL of as-synthesized CTAB-GNRs were washed with 3 mL $CHCl_3$, and then 120×10^{-6}L of 3-mercaptopropyltrimethoxysilane, MPS, (10×10^{-3} M in ethanol, calculated to provide about 30 molecules nm^{-2}) was added into the CTAB-GNRs in water under vigorous stirring for 30 min. Thereafter, 3 mL of a $CHCl_3$ solution (10×10^{-3} M) of the DLC silane **4** or ODS was added, followed by 30×10^{-6} L of base (1.0 M NaOH). The two-phase system was vortexed for several minutes until the water phase became colorless and the organic phase turned

to red-brown, indicating the functionalization to LC-functionalized, hydrophobic GNRs. The organic layer was separated and the GNRs was isolated by centrifugation (12 000 rpm, 20 min) and washed with toluene.

3. Results and Discussion

Figure 1a shows the schematic representation of the as-synthesized **DLC-GNR**s and Figure 1b shows the UV–Vis–NIR absorbance spectrum of the DLC-GNRs in chloroform. The absorption bands at 520 and 820 nm belong to the transversal and longitudinal surface plasmon resonance (SPR) absorbances of the DLC-GNRs, respectively, indicating that the aspect ratio of the GNRs is about 3–4 on average.[19] Moreover, the absorbance bands at 250–290 nm belong to the valence electron π–π^* transition of the triphenylene core of the DLC molecules. The peak of this band shifted from 285 nm for the free DLC molecules (blue spectrum in Figure 1b) to 260 nm for the GNRs dispersion (red spectrum in Figure 1b). This slight blueshift can be explained by the local field enhancement near the surface of the GNRs,[20] and was used as an evidence for the DLC molecules attachment to the surface of the GNRs. The 2D-simplified cartoon of the **DLC-GNR**s in Figure 1a also highlights that during the silane conjugation a small amount of CTAB surfactant is retained on the surface of the GNRs as established in previous work using X-ray photoelectron spectroscopy.[10,17]

The self-assembly behavior of the neat **DLC-GNR**s on substrates was first investigated by drop casting dispersions of the GNRs in toluene on carbon-coated TEM copper grids after slow evaporation of the solvent. **Figure 2** shows some representative TEM images of the **DLC-GNR** samples dried from GNRs dispersion in toluene (about 6 mg mL^{-1}). Instead of an even, yet random dispersion on the grid during the solvent evaporation, the DLC-functionalized GNRs tend to gather together in a side-by-side fashion to form what is best described as ribbons of nanorods.

The self-assembly potential of the **DLC-GNR** supported by these images suggests that there are attractive interactions between the GNRs driving the side-by-side long-range assembly. In this case, the major driving forces are π–π interactions between the triphenylene moieties of the DLC molecules in addition to natural side-by-side assembly of anisometric rod-like entities. As sown in **Figure 3**, these assemblies exist over very large areas with several μm^2 dimensions.

To obtain a monolayer of GNRs on the TEM grid that allows us to measure the distance between neighboring GNRs, we also tuned the concentration of the GNRs dispersion. The image in **Figure 4**a and the corresponding cross section profile (Figure 4b) shows that the gap between **DLC-GNR**s is about 7 nm on average (peak widths were measured as the full width at half maximum), which matches perfectly with the length of the stacking molecules from neighboring GNRs with the triphenylene core overlapping each other (see inset, Figure 4a). For comparison, ODS-coated GNRs were also synthesized, and a representative TEM image of the **ODS-GNR**s drop cast and dried from toluene is shown in Figure 4c. From the corresponding cross sectional profile (Figure 4d), the gap between the ODS-GNRs was measured to be 3–4 nm, which

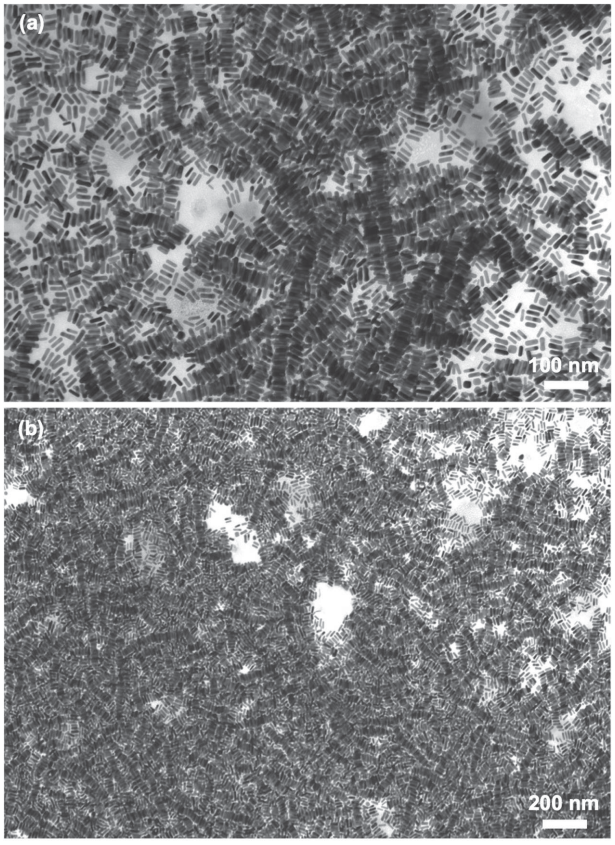

Figure 2. Transmission electron microscopy images of the **DLC-GNR**s dried on TEM grids from dispersion in toluene.

also matches with the molecular length of the alkyl chains of neighboring GNRs overlapping with one other. The key difference is that instead of the large-area assembly of DLC-GNRs presented in Figures 2 and 3, the ODS-GNRs are showing only short-range self-assembly (Figure S1, Supporting Information). It is well known that the self-assembly of anisotropic colloidal nanostructures is to a large extent determined by the type and nature of the surface modification, in other words, a tailored interaction between the rod-like nanoparticles. The DLC molecules themselves, owing to their intrinsic packing in columnar stacks forming a hexagonal columnar phase in a certain

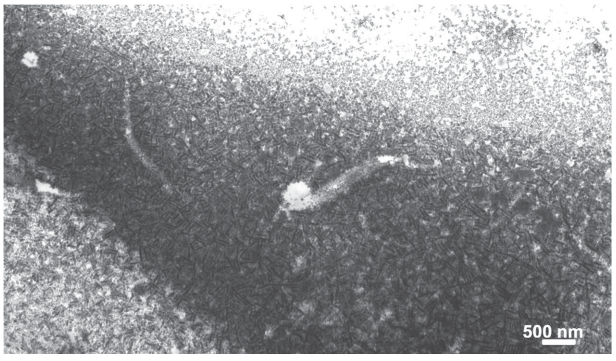

Figure 3. TEM image showing the large-area self-assembly of the **DLC-GNR**s. Several GNR ribbons extend over several hundred nanometers.

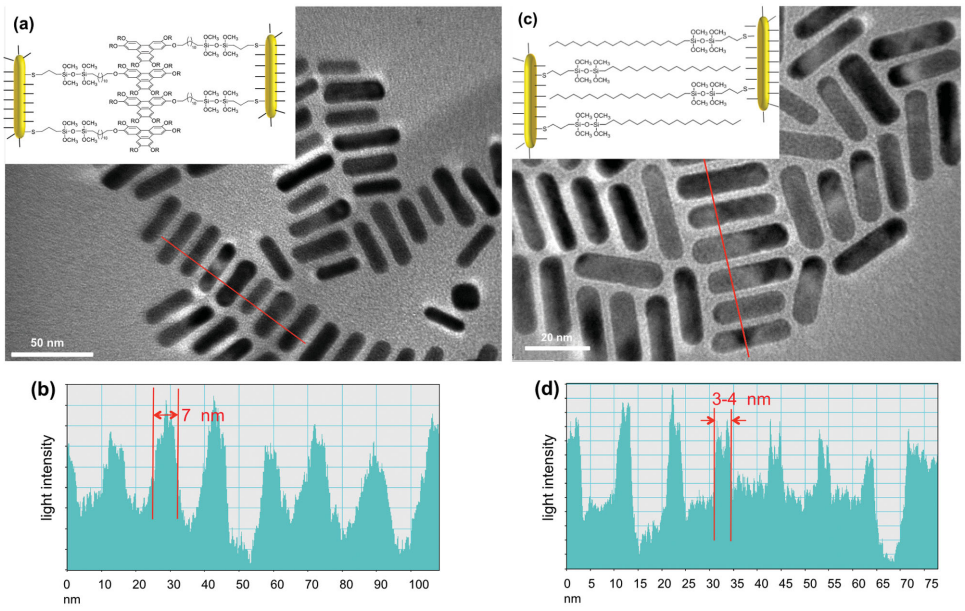

Figure 4. a) TEM image of the **DLC-GNR**s, b) cross section profile of (a), c) TEM image of the **ODS-GNR**s, d) cross section profile of (c). Insets show the arrangement of the GNRs in each case.

temperature interval due to strong π–π stacking, drive here the self-assembly of the GNRs.

To further demonstrate the π–π stacking assembly model inside the multiple layers of the **DLC-GNR**s, a highly condensed dispersion of these GNRs was prepared and drop casted on a Kapton® substrate and dried under ambient atmosphere before performing small-angle X-ray scattering (SAXS) experiments. **Figure 5**a shows the 2D scattering pattern from the X-ray detector. The plot of intensity versus scattering vector q (Figure 5b) shows a broad peak at $q = 0.035$, corresponding to a d spacing of about 18 nm ($d = 2\pi/q$, in Å), which corresponds to the fast Fourier transform obtained from the TEM images (for example fast Fourier transform (FFT) in Figure 5b obtained from the TEM image shown in Figure 2b using Image J®). Considering the average diameter of the GNRs (11 ± 1 nm), the average gap between **DLC-GNR**s is approximately 7 nm, which agrees perfectly with the number measured by analyzing TEM images, as well as the bimolecular length of the DLCs with overlapping triphenylene cores.

While the large-area self-assembly of the DLC-GNRs on TEM grids is static, the essential π–π interactions should also facilitate alignment of the GNRs in a parent triphenylene host. To study this, we prepared mixtures of the **DLC-GNR**s in two triphenylene-based hexagonal columnar LC hosts, H6TP forming a Col_{ho} (ordered hexagonal columnar) and H4TP forming a Col_{hp} (hexagonal columnar plastic) phase, with the concentrations of the **DLC-GNR**s at 1 or 2 wt% (much higher than reported for many other nanorods in LCs).[21] This concentration will determine the numerical ratio between the H6TP (or H4TP) molecules and the DLC-GNRs. Assuming approximately 7×10^6 free H6TP molecules per GNR (at 1 wt% and 10 mg H6TP) in a given mixture, the ratio between free H6TP molecules and anchored discotic mesogens on the GNR surface is about 1160:1, considering there are approximately 6000 DLC silane molecules attached to the surface of each **DLC-GNR** (with 10% CTAB) following calculations published by Gelbart and co-workers[22] The **DLC-GNR**s easily disperse in the parent DLC hosts (H6TP) without showing any discernable aggregation under the polarized light optical microscope (even at 100× magnification). The thermal behavior observed by differential scanning calorimetry (DSC) measurements (Supporting Information Figure S2 for H6TP)

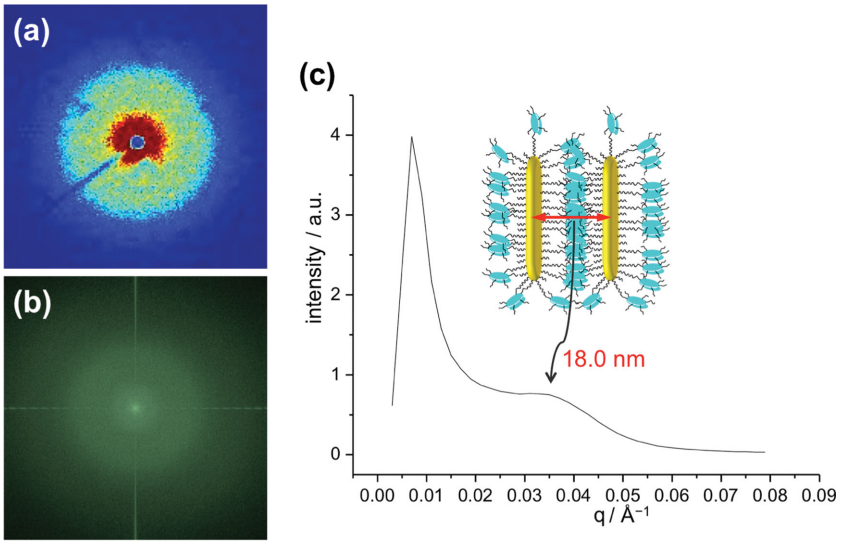

Figure 5. a) 2D SAXS pattern, b) Fourier transform of the TEM image shown in Figure 2b, and c) azimuthally averaged intensity data of the scattering vector (q in $Å^{-1}$) from (a).

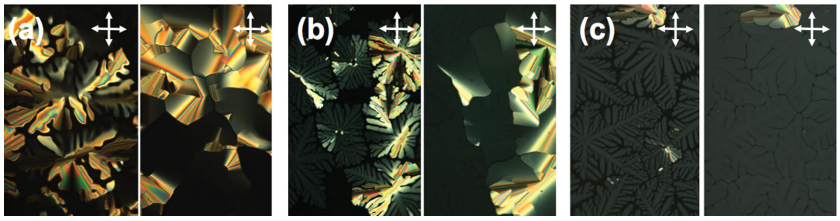

Figure 6. POM photomicrographs (crossed polarizers) taken on cooling at 1 °C min^{-1} of: a) neat H6TP at 99 °C (left) and 88 °C (right), b) H6TP doped with 1 wt% **DLC-GNR**s at 98 °C (left) and 85 °C (right), and c) H6TP doped with 2 wt% **DLC-GNR**s at 96 °C (left) and 85 °C (right).

shows that the LC-phase transition temperatures are practically identical for the pure hosts and the 1 and 2 wt%-doped samples during both heating and cooling runs (Supporting Information Table S1 for H4TP).

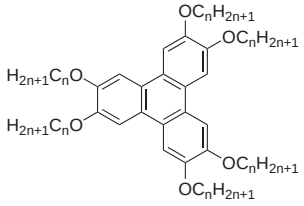

n=4 **H4TP**; Cr 85.6 Col_{hp} 144 Iso
n=6 **H6TP**; Cr 67.6 Col_{ho} 99.0 Iso

At first, temperature-controlled polarized light optical microscopy (POM) was performed, as this technique always provides the first clues if a particular nanomaterial tends to aggregate in a LC-host phase. For the given **DLC-GNR**s no such tendency was observed and aggregates that may eventually form at the higher concentration are not visible at magnifications up to 100×. For H6TP, the texture observed by POM for neat H6TP appear virtually unaltered after the addition and dispersion of the **DLC-GNR**s. **Figure 6**a–c shows the typical dendritic (right at the transition from Iso to Col_{ho}) and mosaic-type textures (deeper into the Col_{ho} phase) textures for neat H6TP and H6TP doped with 1 and 2 wt% **DLC-GNR**s.

Similar overall trends were also observed for H4TP during POM analysis as shown in **Figure 7**. For H4TP, however, highly birefringent (and rather colorful) textures were observed on cooling in a very narrow temperature interval (≈1 °C–2 °C) immediately at the transition from the isotropic liquid to the Col_{hp} phase. Similar textural features have previously been described for tilted, supramolecular chiral (or racemic) columnar phases, and may provide the first hint for a potentially induced tilt after inclusion of the GNRs into the hexagonal lattice of the two hosts.

First, however, we wanted to test if the more fluid Col_{ho} of H6TP could be used to macroscopically align the **DLC-GNR**s, a critical aspect for the use of anisometric metal nanorods in potential applications as optical-phase retarders or wave plates. To study this in a rather simple approach, the 1 wt% **DLC-GNR**s-doped H6TP sample was placed between two plain glass slides, and planar alignment of the Col_{ho} phase of H6TP was achieved by shearing the cover slide in one direction at a temperature of 85 °C. POM images of the alignment obtained for this cell are shown in **Figure 8**. Under crossed polarizers, when the shearing direction was parallel to the polarizer (director *n* of the aligned H6TP molecules, yellow arrow), the aligned cells gave the weakest birefringence (Figure 8a). The birefringence reached the maximum when the shearing direction was 45° with respect to both polarizers (Figure 8b) indicating the planar alignment of H6TP in these nontreated cells. In order to investigate the orientation (alignment) of the

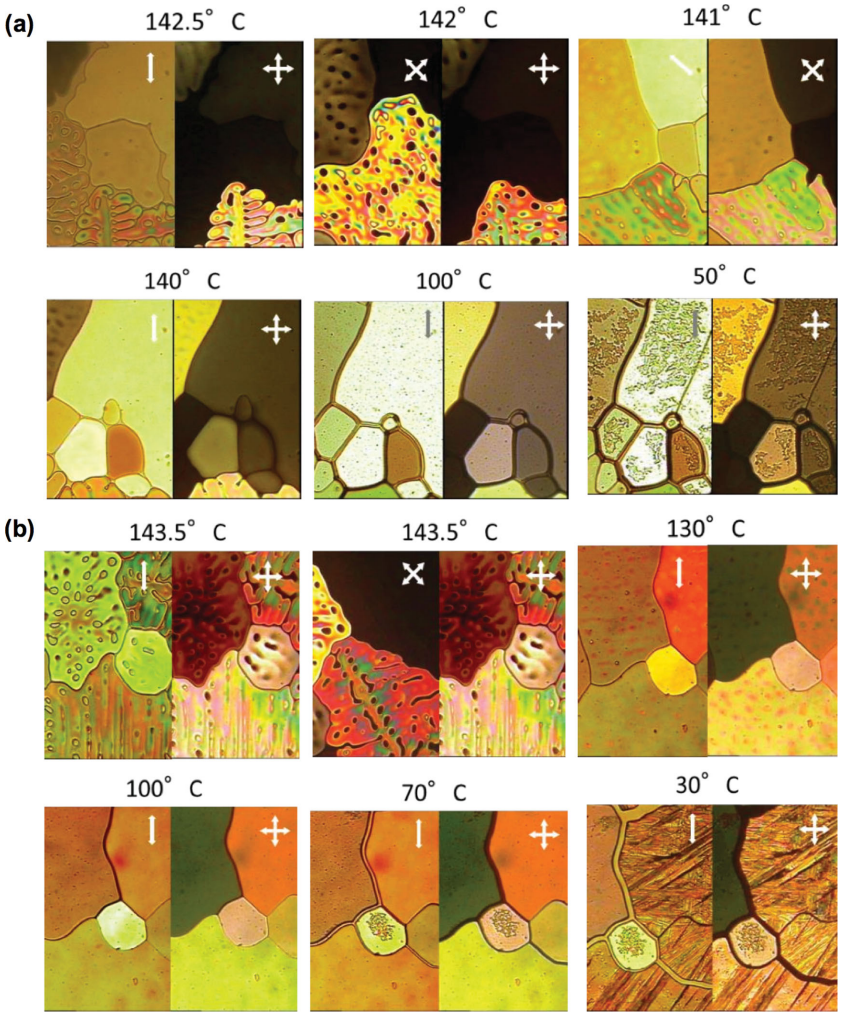

Figure 7. POM photoimages taken on cooling at 1 °C min^{-1} (left: uncrossed polarizers; right: crossed polarizers): a) H4TP doped with 1 wt% **DLC-GNR**s and b) H4TP doped with 2 wt% **DLC-GNR**s at various temperatures. Within a very narrow temperature interval on cooling, highly birefringent and colorful textures are seen immediately below the isotropic liquid phase.

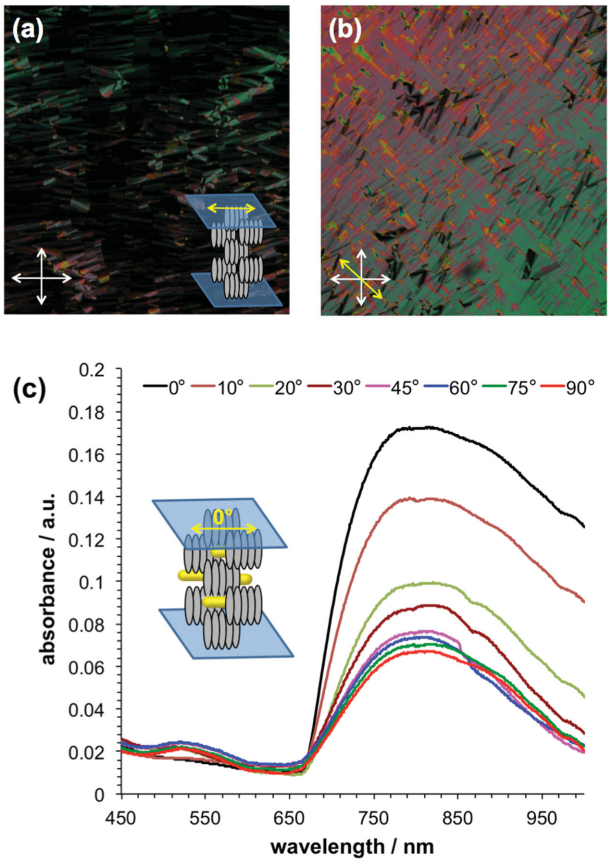

Figure 8. a,b) Polarized optical images of the planar alignment cell of H6TP doped with 1 wt% of **DLC-GNR**s, c) polarized UV–Vis–NIR spectra of the **DLC-GNR**s doped in H6TP (planar-aligned cell) at different polarizer rotation angles.

DLC-GNRs doped in the superstructure of H6TP, the planar-aligned cell was studied using linearly polarized UV–Vis–NIR spectrophotometry. From the spectra of the polarized absorption experiments (Figure 8c), the absorbance band at around 800 nm corresponding to the longitudinal SPR of the GNRs is tunable by rotating the planar-aligned thin Col_{ho} film. The intensity of this band decreased when the angle between polarizer and the director *n* is rotated from 0° to 90° and reaches the minimum intensity at 90°, while the polarization of the beam is perpendicular to the transversal direction of the **DLC-GNR**s. This is in principle also true for the transversal SPR band centered around 535 nm (zero absorbance at 0° and 10°, maximum absorbance at 90°; 45° making the logical exception), which indicates that the majority of the **DLC-GNR**s in the aligned cell follows the director *n* with their long axes a shown in the insert of Figure 8c.

The polarized UV–Vis–NIR spectrum at 90° shows as expected the weakest absorbance at 800 nm, but not zero, which means that the alignment of H6TP is not perfect (as can actually be seen in Figure 8a), but potentially also that a portion of the GNRs is not perfectly aligned along the director. As one can see from Figure 8a, some areas still have weak birefringence, and appear as bright domains. The order parameter *S* of the **DLC-GNR**s can be calculated using the following equation[23]:

$$S = \frac{A_{\parallel} - A_{\perp}}{A_{\parallel} + 2A_{\perp}}$$

where $A_{\parallel}$ and $A_{\perp}$ is the absorbance measured with the polarizer either parallel or perpendicular to the director *n*, respectively. The resulting order parameter *S* (dichroic ratio) was calculated to be 0.38. Considering that the typical order parameter of planar alignment of columnar phase of discotic LCs achieved by mechanical shearing[24] is in the vicinity of 0.5, the **DLC-GNR**s inserted into the planar alignment columnar phase are aligned along the director *n* with an over 75 % efficiency.

With POM and UV–Vis–NIR experiments suggesting that the **DLC-GNR**s are reasonably well dispersed in the hexagonal columnar LC phases of both H4TP and H6TP, we sought to determine if the suspended GNRs have any effect on the organization and structure of the host phase by performing medium and wide-angle X-ray diffraction experiments. While we have not been able to pinpoint and carefully study the potential high-temperature modification exhibiting the bright, highly birefringent textures for the 1 and 2 wt% **DLC-GNR** in H4TP mixtures (too narrow temperature interval), the obtained X-ray diffraction data did reveal some rather unique trends when both hosts are doped with the **DLC-GNR**s. In both cases, we selected the same temperature well below the Iso/Col_h phase-transition temperature (since DSC and POM revealed no thermal effect of the addition of the **DLC-GNR**s in the two hosts) on cooling (80 °C for H6TP and 125 °C for H4TP) and collected X-ray diffraction data, which are shown in **Figure 9** and summarized in **Table 1**.

First, the diffraction pattern of both pure H6TP and H4TP perfectly match data published previously.[25] Second, the packing of H4TP appears to be more significantly impacted by the dispersion of the **DLC-GNR**s than H6TP at least judging from the plot of the scattering intensity versus *q*, with some of the (311)/(320) diffraction peaks disappearing and a completely altered intensity profile. The calculated data for the *d* spacing and the lattice parameter a_{hex} (from d_{100}), however, indicate that there is only a minor decrease in a_{hex} for H4TP, but a significant decrease for H6TP both doped with 1 wt% **DLC-GNR**s, but not for the 2 wt%-doped sample. While one would expect an increase in *d* spacing (and lattice parameter)[26] upon insertion of GNRs with a much larger diameter, the lattice parameter for the 1 wt% **DLC-GNR**s in H6TP sample decreases by about 8%, which at this point could only be explained by a more efficient interdigitation of the alkyl chains surrounding the triphenylene cores of H6TP. Here, the insertion of the GNRs might lead to packing mismatch between DLC molecules attached to the GNR surface and DLC molecules of the host. At the volume fraction of 1 wt% of **DLC-GNR**s in H6TP, such packing mismatch could lead to packing frustration that might be compensated by a larger degree of interdigitation. Such process, however, would be more pronounced with H6TP than H4TP because of the longer hydrocarbon chains (see schematics in **Figures 10** and **11**). Such interdigitation would be less significant for H4TP because of the shorter chain length, which is supported by the less significant decrease in *d* (and a_{hex}) for H4TP doped with 1 wt% **DLC-GNR** (see Table 1). For H4TP this packing frustration reaches its maximum at 2 wt% **DLC-GNR**s indicated by a decrease of a_{hex} to 1.93 nm (a 6% decrease).

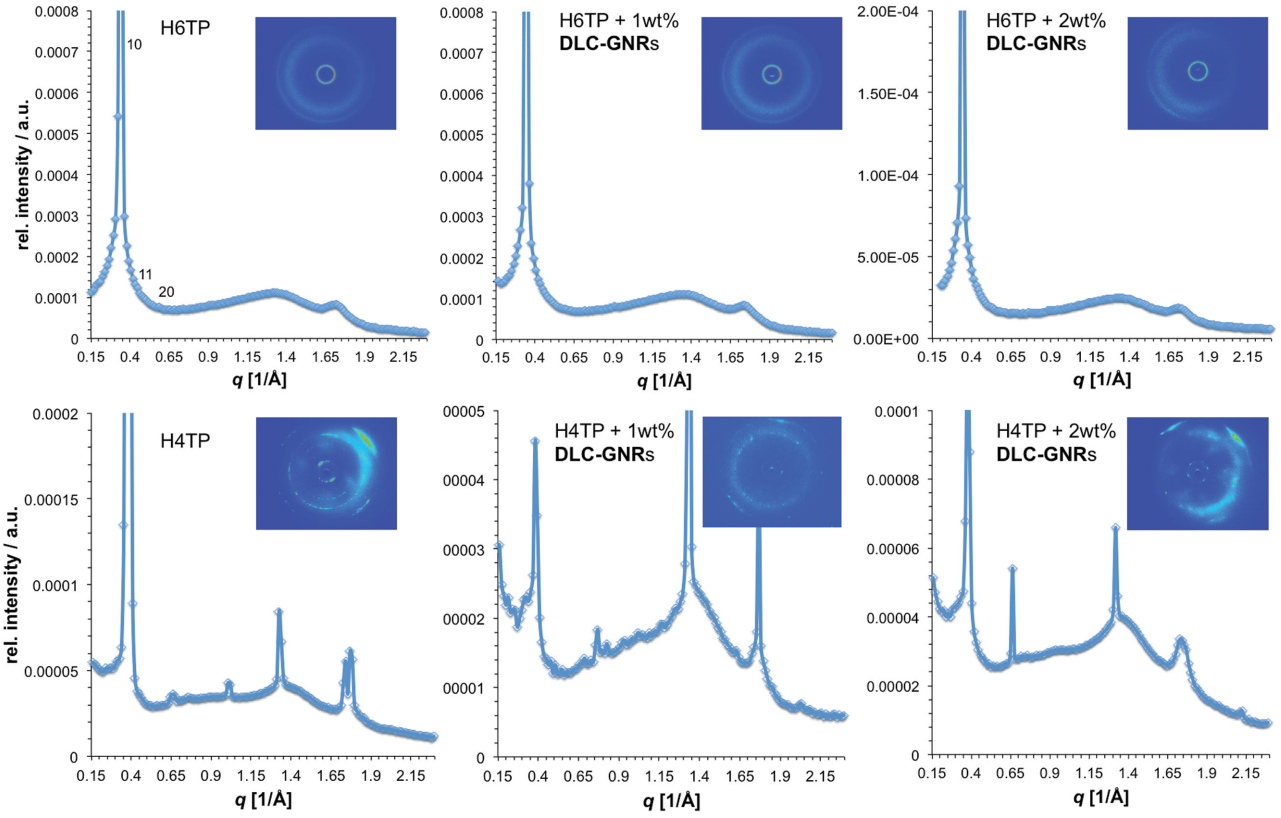

Figure 9. X-ray diffraction pattern and azimuthally averaged intensity data of the scattering vector (q in Å^{-1}) from the 2D pattern shown as insets.

The intracolumnar spacing however remains virtually identical. For H6TP, both the intracolumnar distance between the molten alkyl chains and the core–core distance simultaneously decreases, most considerably for the 1wt%-doped H6TP, with a core–core distance decrease from 0.379 to 0.367 nm. However, once the concentration of the **DLC-GNR**s is doubled to 2 wt%, most likely an onset of aggregation of the GNRs minimizes these packing effects and the lattice relaxes back to the values of the nondoped H6TP host phase. Another possibility to explain a decrease of both a_{hex} and core–core distance would be a molecular tilt of the molecules within the columns (23° to be exact), but this can be ruled out as the resulting phase would have a different symmetry. Such molecular tilt would give rise to an elliptical cross section of the columns leading to an assignment as a rectangular columnar phase (Col_r). In neither case do the powder XRD pattern support such phase symmetry and assignment. However, the insertion of the GNRs, at least at lower volume fractions induces a tighter packing of the host molecules both inter- and intracolumnar at 1 wt% for H6TP, which should give rise to a higher charge carrier mobility in these phases, which we tested next using transient photocurrent measurements using the TOF technique.[14] For H4TP exclusively the intercolumnar packing decrease at 2 wt% **DLC-GNR**s, which should in principle not affect the charge carrier mobility unless other electronic processes or ionic contributions are active.

These measurements require extremely pure samples and ideally excellent homeotropic alignment in thin, ITO-coated cells (cell gap: 2–3 µm), and the most reliable data sets were acquired for the ultrapure H4TP synthesized and purified previously by Shimizu and co-workers.[25] The use of thin cells for TOF measurements shows a direct effect on the alignment of the **DLC-GNR** composites. While we were unable to obtain complete homeotropic alignment in cells with a ≈15 µm cell gap, it occurred spontaneously for the 1 wt% **DLC-GNR**/H4TP composite in the ≈3 µm thin cell, and remained present throughout the whole temperature range analyzed on cooling (from 141 to 20 °C). The 2 wt% composite also shows homeotropic regions albeit significantly smaller (see Figure S3, Supporting Information). The presence of homeotropic regions in the **DLC-GNR**s composites contributes to the enhancement of the hole mobility as it reflects an increased uniaxial ordering along the columnar axis that is absent in the pure H4TP sample.

Figures 12 and **13** show the obtained transient photocurrent decay curves for both hole and electron transports for H4TP doped with 1 and 2 wt% **DLC-GNR**s and H6TP doped with 1 wt% **DLC-GNR**s (hole mobility only). H4TP and H6TP are known to show ambipolar character for the charge transport in electronic processes,[27] and in comparison to those of the pure, undoped compounds, the GNR-doped systems tend to show noisy and less qualified decay curves, although an electric field-independent character of the mobility is still observed (see Figure S4, Supporting Information). This may indicate that local disordering of the discotic molecules is induced by the addition of the surface modified **DLC-GNR**s. H4TP and

Table 1. Measured scattering vectors (q in Å^{-1}) with respective Miller indices, and calculated d spacing as well as lattice parameters of the Col_h phase in nm. The intracolumnar distance refers to the distance between molten hydrocarbon chains, the core–core distance to the distance between the triphenylene cores within the columnar aggregates.

Sample	T [°C]	$q_{(hkl)}$ [Å^{-1}]	d [nm]	a_{hex} [nm]	Stacking periodicities [nm]	
					Intracolumnar	Core–Core
H6TP	80	$q_{(100)} = 0.3218$	1.953	2.252	0.495	0.379
		$q_{(110)} = 0.5447$				
		$q_{(200)} = 0.656$				
		$q = 1.27$				
		$q = 1.66$				
H6TP + 1 wt% **DLC-GNRs**	80	$q_{(100)} = 0.3485$	1.803	2.082	0.477	0.367
		$q_{(110)} = 0.614$				
		$q = 1.316$				
		$q = 1.714$				
H6TP + 2 wt% **DLC-GNRs**	80	$q_{(100)} = 0.3231$	1.945	2.246	0.491	0.379
		$q_{(110)} = 0.608$				
		$q = 1.28$				
		$q = 1.658$				
H4TP	125	$q_{(100)} = 0.3539$	1.775	2.05	0.479	0.358
		$q_{(110)} = 0.645$				
		$q_{(200)} = 0.7148$				
		$q_{(210)} = 0.992$				
		$q_{(220)(211)} = 1.311$				
		$q_{(311)(320)} = 1.728$				
		$q_{(002)} = 1.7557$				
H4TP + 1 wt% **DLC-GNRs**	125	$q_{(100)} = 0.3673$	1.711	1.975	0.475	0.358
		$q_{(110)} = 0.6307$				
		$q_{(200)} = 0.7415$				
		$q_{(220)(211)} = 1.324$				
		$q_{(002)} = 1.7534$				
H4TP + 2 wt% **DLC-GNRs**	125	$q_{(100)} = 0.3759$	1.672	1.93	0.476	0.363
		$q_{(110)} = 0.6629$				
		$q_{(200)} = 0.7176$				
		$q_{(210)} = 0.95$				
		$q_{(220)(211)} = 1.319$				
		$q_{(311)(320)} = 1.729$				
		$q_{(002)} = 1.7564$				

H6TP both exhibit hexagonal columnar (Col_h) phases, however with a slight difference in the molecular ordering. The shorter chain homologue, H4TP shows a 3D-plastic columnar phase with a 2D hexagonal arrangement of columns (Col_{hp} phase),[28] whilst H6TP displays a Col_{ho} mesophase with some degree of ordering along the columnar axis (see X-ray diffraction data in Figure 9). Their hole and electron mobilities are recorded on the order of 10^{-2} and 10^{-4} cm^2 V^{-1} s^{-1} for the Col_{hp} and the Col_{ho} phase, respectively, and both show largely temperature-independent character.[25] The temperature dependencies of the charge carrier mobility for the two composites of H4TP are depicted in **Figure 14**. All essentially show a temperature-independent nature for both holes and electrons except for a sudden jump at about 115 °C for the electron mobility. There

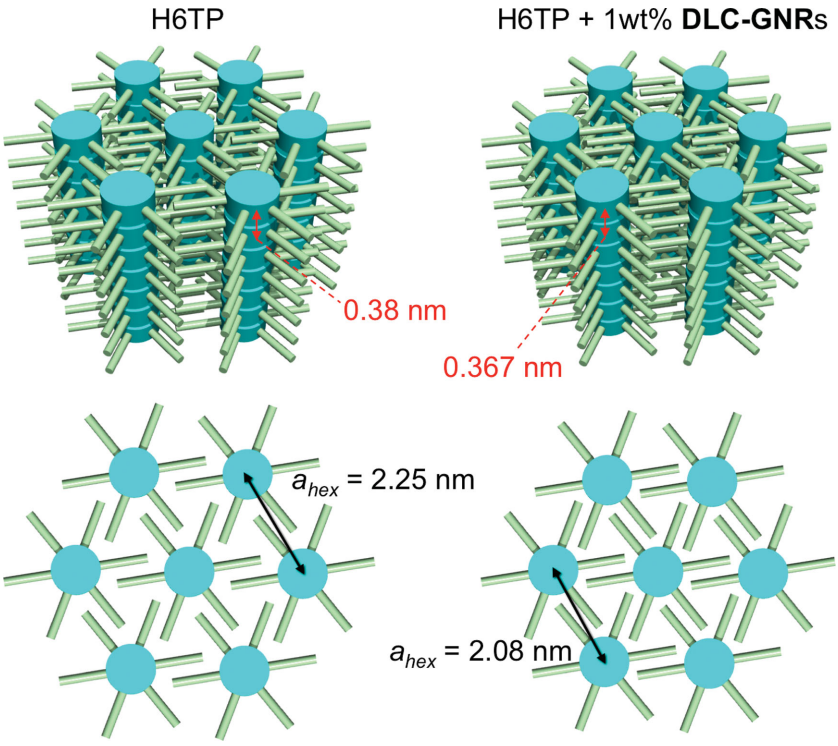

Figure 10. Schematic of the Col_{ho} phase of H6TP and H6TP doped with 1 wt% **DLC-GNRs** showing the decrease in lattice parameter as well as intracolumnar packing.

is no evidence of a phase transition, although an optical texture change indicates a potential phase or structure modification within these domains around this temperature (see Figure 14b). This change in the optical textures is best described by a slight widening of the domain boundaries (Figure 7), although DSC measurements show no first order phase transition in this temperature range. Interestingly, this sudden change in mobility is not seen for the hole mobility, which drops for the 2 wt% mixture, likely due to an onset of aggregation of the DLC-GNRs in H4TP, but otherwise increases below the Cr/Col_{hp} phase transition (rather than decrease for neat H4TP). Overall, the mobilities of both holes and electrons are comparable to those of pure H4TP in the LC phase, and the mixture of 1 wt% DLC-GNRs in H4TP shows a slightly higher value of the mobility. This may indicate that the optimal concentration of the **DLC-GNRs** would exist around this concentration

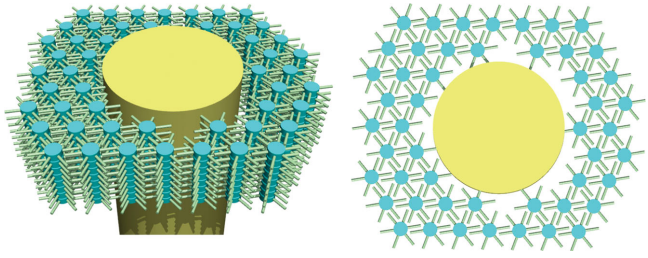

Figure 11. Schematic of the H6TP (or H4TP) doped with 1 wt% **DLC-GNRs** (3D and top 2D view) showing potential packing inefficiencies around a single-DLC-capped GNR that are potentially compensated as determined by XRD.

and provide the maximum mobility. For the 1wt% **DLC-GNR** composite with H6TP, the mobility behavior is similar to those of the composites with H4TP. Here, the measured hole mobility measured for the composite is slightly higher than the one of pure H6TP (≈3.2 × 10^{-4} cm^2 V^{-1} s^{-1} for the composite vs 2.0 × 10^{-4} cm^2 V^{-1} s^{-1} f or neat H6TP over the Col_{ho} mesophase range.[25] The carrier mobilities obtained for undoped H4TP as well as the composites with **DLC-GNR** are summarized in **Table 2**, and the data for H6TP are collected in the Supporting Information (POM and hole mobility, see Figure S5, Supporting Information).

Kumar et al. reported on an enhancement of the conductivity with the inclusion of GNRs (1 wt% for H5TP) from 10^{-9} to 10^{-6} Sm^{-1}, which was even higher than in the isotropic liquid phase (10^{-7} Sm^{-1}).[26,29] A related enhancement of the conductivity was also reported for composites with gold nanoparticles dispersed in H6TP.[30] The conductivity is a function of the number of efficient charges in the system and their mobility. Enhancement of the conductivity is thus the result of an increased number of carriers mobile in the system and/or improved mobility of the charge carriers. Hence, in both composites of 1 and 2 wt% **DLC-GNRs** in H4TP, the enhanced conductivity reported is best explained by an increase in the number of efficient charges. If we assume that the charge conduction in this system is only arising from electronic processes, the doping of GNRs would have to elevate the number of charges. On the other hand, conductivity phenomena essentially include ionic transport processes. In particular, soft states of matter such as LC phases sometimes provide a good ionic charge transport path.[31] Considering that the mobilities measured using the TOF technique are rather high in comparison to those of ionic mobility, and that the temperature dependence obeys Arrhenius formalism, the enhanced conductivity is probably derived from charge transport in ionic processes.

4. Conclusions

In continuation of our earlier experiments on the reconfigurable self-assembly of nematic LC-capped GNRs,[10,17] we here demonstrate that GNRs functionalized with DLC π–π stacking motifs also foster long-range, bulk self-assembly and permit alignment in a parent DLC host. The as-synthesized **DLC-GNRs** can be homogeneously dispersed in organic solvents, such as toluene and chloroform, at fairly high concentrations. These dispersions, dried on TEM grids, flat substrates, or in the bulk show large-area self-assembly of the as observed by TEM and SAXS. However, true liquid crystalline behavior could not be observed. The proposed stacking assembly model is supported by distance measurements using TEM image

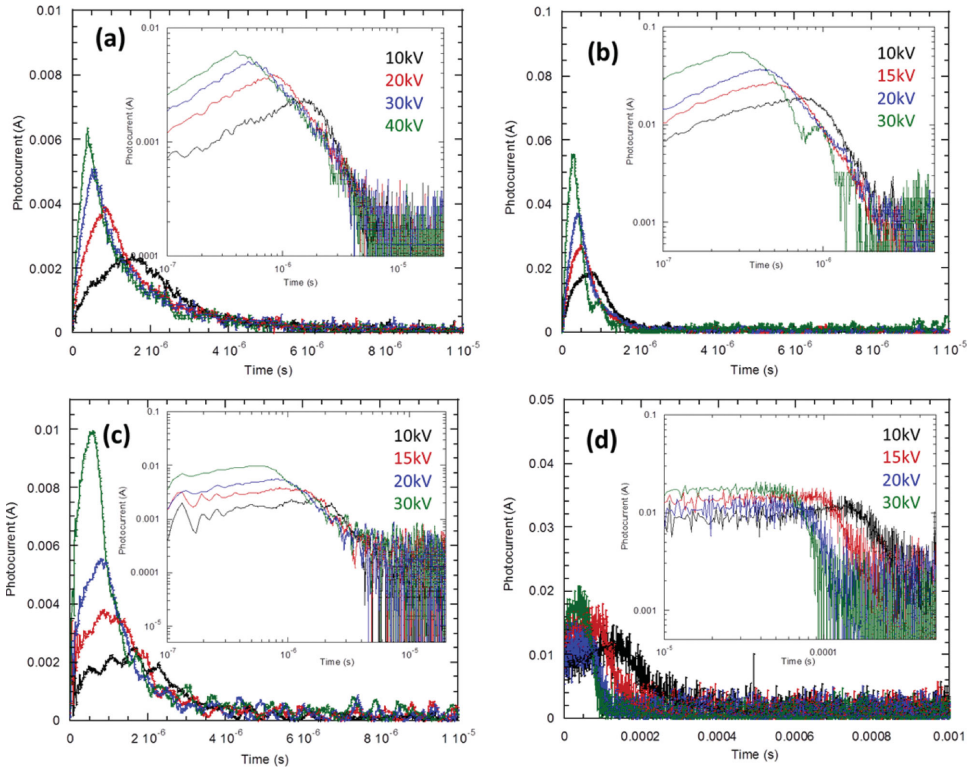

Figure 12. Bias dependence of the hole mobility of: a) pure H4TP, b) 1 wt% **DLC-GNR**s in H4TP, c) 2 wt% **DLC-GNR**s in H4TP (all three at 140 °C in the Col_{hp} phase), and d) 1 wt% **DLC-GNR**s in H6TP (at 90 °C in the Col_{ho} phase).

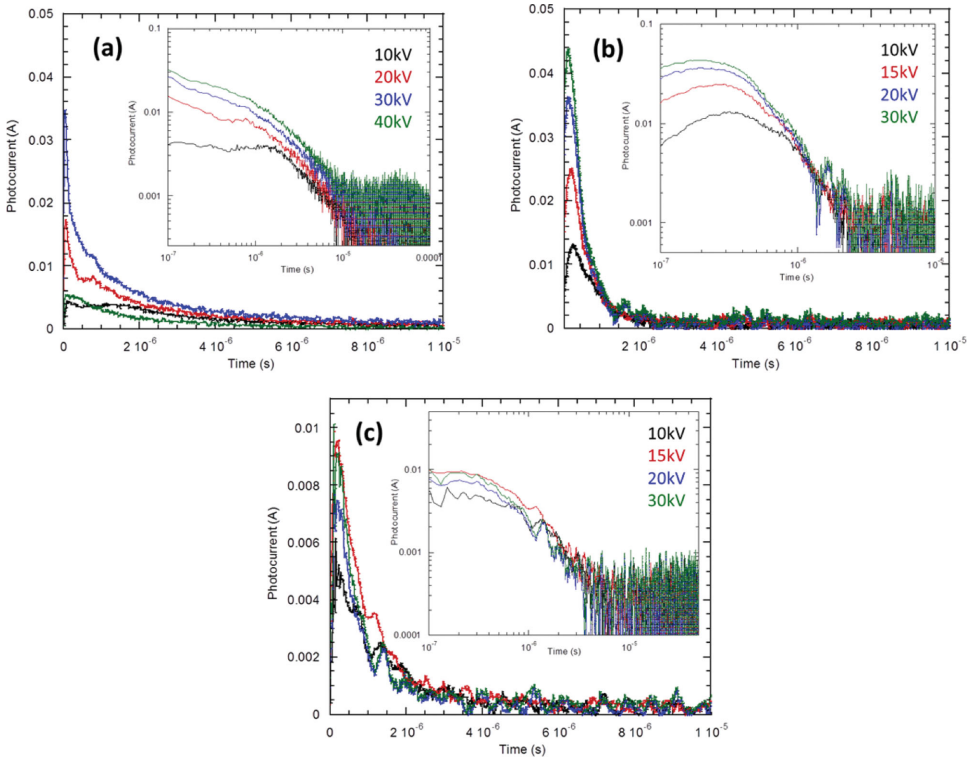

Figure 13. Bias dependence of the electron mobility of: a) pure H4TP, b) 1 wt% **DLC-GNR**s in H4TP, c) 2 wt% **DLC-GNR**s in H4TP (at 140 °C in the Col_{hp} phase).

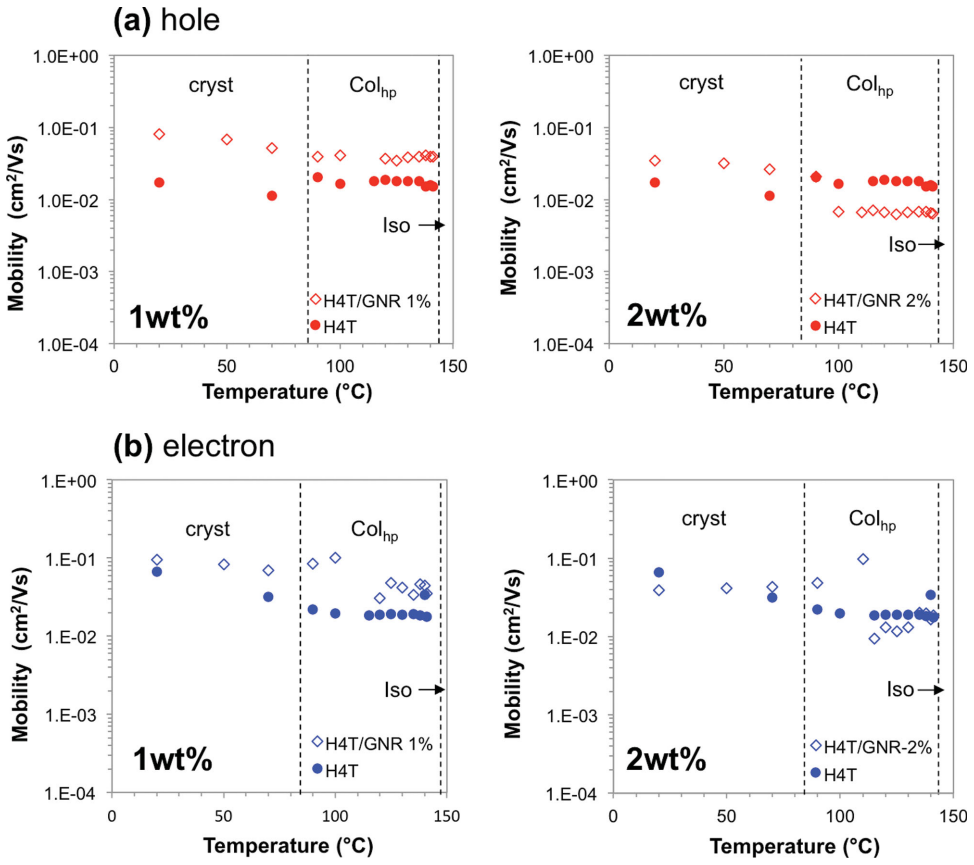

Figure 14. Temperature dependence of hole and electron mobilities for: a) 1 wt% and b) 2 wt% **DLC-GNR** in H4TP at 10 kV cm^{-1}.

analysis and SAXS showing identical distances between side-by-side self-assembled GNRs based on π–π molecular stacks between neighboring GNRs. In combination with our earlier data regarding the distances between nematic LC-functionalized GNRs,[10] the interparticle distance, i.e., the coupling effect,[32] can be fine tuned by the LC-packing mode, which shows promise for potential application as metamaterials or field-enhanced spectroscopy units in electric and optical nanodevices.[11,33] Furthermore, we have demonstrated that the DLC-functionalized GNRs are compatible with the parent DLC hosts. The enhanced thermal stability provided by the silane conjugation approach allows us to disperse these DLC-capped GNRs without the risk of thiol desorption from the GNR surface eliminating the risk of free thiols contributing both positively or negatively to the observed effects. Homogeneous dispersion and uniform alignment of the DLC-functionalized GNRs have been achieved in a planar-aligned H6TP DLC host over areas as large as several cm^2, employing a very simple and well-established alignment technique for DLCs without any applied electric or magnetic field. These composites show rather unique structural features particularly at the lower concentration of 1% by weight. SAXD data reveal that the lattice parameter decreases from 2.25 to 2.08 nm for the host featuring longer hydrocarbon chains (H6TP) at 1 wt% of dispersed GNRs and relaxes back to 2.25 nm when the concentration of the GNRs is doubled, likely indicating the onset of some GNR aggregation. This effect is more pronounced for the less viscous H6TP forming the Col$_{ho}$ phase in comparison to the more viscous H4TP forming a plastic Col$_{hp}$ phase. Simultaneously, the intracolumnar distances also decrease at the lower concentration of GNRs especially in H6TP, which gives rise to an increase in the charge carrier mobility for both electrons and holes. These results indicate that the inclusion of the **DLC-GNR**s into the hexagonal columnar LC affects the charge transport efficiency only slightly at the lower concentration range of dispersed GNRs. However, the interdigitation of columnar semiconductors and functionalized metal nanorods as conducting active parts and electrodes, respectively, may provide a simple yet effective strategy for organic photovoltaics.

Table 2. Carrier mobility for H4TP and H4TP doped with 1 and 2 wt% **DLC-GNR**s.

Sample	Charge carrier mobility [10^{-2} cm^2 Vs^{-1}]			
	Hole		Electron	
	Col$_{hp}$	Cr	Col$_{hp}$	Cr
neat H4TP	1.7	1.4	2.0	4.9
H4TP (1 wt% **DLC-GNR**s)	3.9	6.7	5.2	8.2
H4TP (2 wt% **DLC-GNR**s)	0.7	3.1	2.4	4.1

Supporting Information

Supporting Information is available from the Wiley Online Library or from the author.

Acknowledgements

The authors would like to thank the Province of Manitoba for a grant from the Science and Technology International Collaboration Fund, the Centre for Chemical Innovation (CCI) (Caltech), the Natural Science and Engineering Research Council (NSERC) of Canada, the Canada Foundation for Innovation (CFI), and the Manitoba Research and Innovation Fund (MRIF) for financial support. TH also acknowledges financial support from Kent State University and the Government of Ohio's Third Frontier Program for Ohio Research Scholars. T.M. is grateful for financial support through a JSPS fellowship. L.S. and Y.S. acknowledge JST for the finical support under the ALCA program. Special thanks go to Dr. Kevin McEleney for his help with the SAXS experiments and to Andre Dufresne for all the help and assistance with TEM imaging.

Received: June 5, 2014
Revised: November 17, 2014
Published online: December 17, 2014

[1] a) T. Hegmann, H. Qi, V. M. Marx, *J. Inorg. Organomet. Polym. Mater.* **2007**, *17*, 483; b) U. Shivakumar, J. Mirzaei, X. Feng, A. Sharma, P. Moreira, T. Hegmann, *Liq. Cryst.* **2011**, *38*, 1495; c) O. Stamatoiu, J. Mirzaei, X. Feng, T. Hegmann, *Top. Curr. Chem.* **2012**, *318*, 331; d) G. L. Nealon, R. Greget, C. Dominguez, Z. T. Nagy, D. Guillon, J. L. Gallani, B. Donnio, *Beilstein J. Org. Chem.* **2012**, *8*, 349–370; e) S. Umadevi, V. Ganesh, T. Hegmann, *Handbook of Liquid Crystals*2nd Ed., (Eds: J. W. Goodby, P. J. Collings, T. Kato, C. Tschoerske, H. F. Gleeson, P. Raynes) Vol. no. *6*, Wiley-VCH, Weinheim, Germany **2014**.

[2] a) M. Grzelczak, L. M. Liz-Marzan, *Langmuir* **2013**, *29*, 4652; b) M. Zorn, R. Zentel, *Macromol. Rapid. Commun.* **2008**, *29*, 922; c) C. M. Soukoulis, S. Linden, M. Wegener, *Science* **2007**, *315*, 47; d) V. M. Shalaev, *Nat. Photonics* **2007**, *1*, 41; e) S. Meuer, P. Oberle, P. Theato, W. Tremel, R. Zentel, *Adv. Mater.* **2007**, *19*, 2073; f) S. Meuer, L. Braun, R. Zentel, *Chem. Commun.* **2008**, 3166; g) A. B. Golovin, O. D. Lavrentovich, *Appl. Phys. Lett.* **2009**, *95*, 254104; h) A. B. Golovin, J. Xiang, H. S. Park, L. Tortora, Y. A. Nastishin, S. V. Shiyanovskii, O. D. Lavrentovich, *Materials* **2011**, *4*, 390.

[3] a) J. J. Zhou, G. X. Chen, E. Wu, G. Bi, B. T. Wu, Y. Teng, S. F. Zhou, J. R. Qiu, *Nano Lett.* **2013**, *13*, 2241; b) T. Wang, X. R. Wang, D. LaMontagne, Z. W. Wang, Y. C. Cao, *J. Am. Chem. Soc.* **2013**, *135*, 6022; c) Y. Zhao, A. Alu, *Nano Lett.* **2013**, *13*, 1086; d) X. P. Li, T. H. Lan, C. H. Tien, M. Gu, *Nat. Commun.* **2012**, *3*, 1.

[4] X. Y. Zheng, J. Fontana, M. Pevnyi, M. Ignatenko, S. Wang, R. Vaia, P. Palffy-Muhoray, *J. Mater. Sci.* **2012**, *47*, 4914.

[5] Y. Q. Wang, B. Yan, L. X. Chen, *Chem. Rev.* **2013**, *113*, 1391.

[6] a) E. V. Shevchenko, D. V. Talapin, N. A. Kotov, S. O'Brien, C. B. Murray, *Nature* **2006**, *439*, 55; b) S. C. Glotzer, M. J. Solomon, *Nat. Mater.* **2007**, *6*, 557.

[7] a) Y. J. Min, M. Akbulut, K. Kristiansen, Y. Golan, J. Israelachvili, *Nat. Mater.* **2008**, *7*, 527; b) K. J. M. Bishop, C. E. Wilmer, S. Soh, B. A. Grzybowski, *Small* **2009**, *5*, 1600.

[8] T. S. Sreeprasad, T. Pradeep, *Langmuir* **2011**, *27*, 3381.

[9] A. Guerrero-Martinez, J. Perez-Juste, E. Carbo-Argibay, G. Tardajos, L. M. Liz-Marzan, *Angew. Chem. Int. Ed.* **2009**, *48*, 9484.

[10] S. Umadevi, X. Feng, T. Hegmann, *Adv. Funct. Mater.* **2013**, *23*, 1393.

[11] M. Yamada, Z. R. Shen, M. Miyake, *Chem. Commun.* **2006**, 2569.

[12] a) S. Kumar, S. K. Pal, P. S. Kumar, V. Lakshminarayanan, *Soft Matter* **2007**, *3*, 896; b) S. Kumar, H. K. Bisoyi, *Angew. Chem. Int. Ed.* **2007**, *46*, 1501.

[13] J. Mirzaei, M. Urbanski, H. S. Kitzerow, T. Hegmann, *Philos. Trans. R. Soc. A* **2013**, *371*, 20120256.

[14] F. Nekelson, H. Monobe, M. Shiro, Y. Shimizu, *J. Mater. Chem.* **2007**, *17*, 2607.

[15] S. Kumar, M. Manickam, *Synthesis-Stuttgart* **1998**, 1119.

[16] a) J. L. Schulte, S. Laschat, V. Vill, E. Nishikawa, H. Finkelmann, M. Nimtz, *Eur. J. Org. Chem.* **1998**, *11*, 2499; b) H. Schonherr, F. J. B. Kremer, S. Kumar, J. A. Rego, H. Wolf, H. Ringsdorf, M. Jaschke, H. J. Butt, E. Bamberg, *J. Am. Chem. Soc.* **1996**, *118*, 13051.

[17] S. Umadevi, X. Feng, T. Hegmann, *Ferroelectrics* **2012**, *431*, 164.

[18] K. Mitamura, T. Imae, N. Saito, O. Takai, *J. Phys. Chem. B* **2007**, *111*, 8891.

[19] B. Nikoobakht, M. A. El-Sayed, *Chem. Mater.* **2003**, *15*, 1957.

[20] S. L. Pan, Z. J. Wang, L. J. Rothberg, *J. Phys. Chem. B* **2006**, *110*, 17383.

[21] M. R. Thomas, S. Klein, R. J. Greasty, S. Mann, A. W. Perriman, R. M. Richardson, *Adv. Mater.* **2012**, *24*, 4424.

[22] D. V. Leff, P. C. Ohara, J. R. Heath, W. M. Gelbart, *J. Phy.s Chem.* **1995**, *99*, 7036.

[23] B. Bahadur, in *Handbook of Liquid Crystals*1st Ed., (Eds: J. W. Goodby, D. Demus, G. Gray, H.-W. Spiess, V. Vill) , Vol. no. *2A*, Wiley-VCH, Weinheim, Germany **1998**.

[24] Q. K. Liu, Y. X. Cui, D. Gardner, X. Li, S. L. He, I. I. Smalyukh, *Nano Lett.* **2010**, *10*, 1347.

[25] H. Monobe, Y. Shimizu, S. Okamoto, H. Enomoto, *Mol. Cryst. Liq. Cryst.* **2007**, *476*, 277.

[26] S. Kumar, *NPG Asia Mater.* **2014**, *6*, e82.

[27] H. Iino, J. Hanna, D. Haarer, R. J. Bushby, *Jpn. J. Appl. Phys.* **2006**, *45*, 430.

[28] J. Simmerer, B. Glusen, W. Paulus, A. Kettner, P. Schuhmacher, D. Adam, K. H. Etzbach, K. Siemensmeyer, J. H. Wendorff, H. Ringsdorf, D. Haarer, *Adv. Mater.* **1996**, *8*, 815.

[29] B. S. Avinash, V. Lakshminarayanan, S. Kumar, J. K. Vij, *Chem. Commun.* **2013**, *49*, 978.

[30] L. A. Holt, R. J. Bushby, S. D. Evans, A. Burgess, G. Seeley, *J. Appl. Phys.* **2008**, *103*, 063712.

[31] a) K. Kishimoto, T. Suzawa, T. Yokota, T. Mukai, H. Ohno, T. Kato, *J. Am. Chem. Soc.* **2005**, *127*, 15618; b) M. Yoshio, T. Mukai, H. Ohno, T. Kato, *J. Am. Chem. Soc.* **2004**, *126*, 994.

[32] K. H. Su, Q. H. Wei, X. Zhang, J. J. Mock, D. R. Smith, S. Schultz, *Nano Lett.* **2003**, *3*, 1087.

[33] a) J. Aizpurua, G. W. Bryant, L. J. Richter, F. J. G. de Abajo, B. K. Kelley, T. Mallouk, *Phys. Rev. B* **2005**, *71*, 235420; b) V. M. Shalaev, W. S. Cai, U. K. Chettiar, H. K. Yuan, A. K. Sarychev, V. P. Drachev, A. V. Kildishev, *Opt. Lett.* **2005**, *30*, 3356.